A miniaturized and flexible optoelectronic sensing system for a tactile skin

L Ascari[1,2], P Corradi[2], L Beccai[3], and C Laschi[2,3]

[1] IMT Doctoral School in Biorobotics, Lucca Institute for Advanced Studies, Lucca, Piazza S. Ponziano, 55100, Italy

[2] CRIM Lab, Scuola Superiore Sant'Anna, Pisa, Piazza Martiri della Libertà 33, 56127, Italy

[3] ARTS Lab, Scuola Superiore Sant'Anna, Pisa, Piazza Martiri della Libertà 33, 56127, Italy

E-mail: luca.ascari@imtlucca.it

Abstract. This paper describes the development of a hybrid sensing module consisting of a general purpose electro-optical converter and three MEMS force sensors, to be integrated into flexible substrates for tactile skin applications. The features of the converter, namely its flexible and thin substrate and small dimensions, programmability, optical coding and transmission of the information allow this versatile device to host different sensors, locally preprocess signals, and transmit information robust to electromagnetic noise. After discussing the major technical requirements, the design of the sensing, electrical and optical subsystems is illustrated, as well as the whole process for its fabrication. A first characterization of a working prototype, hosting three MEMS force sensors and nine independent optical channels was performed: the global performances in terms of sensitivity, bandwidth and spatial sensing resolution make the presented module suitable to be used as basic element of a complete tactile system for robotic applications. Several solutions for mass production, improved optical properties and more efficient optical transmission are discussed.

1. Introduction

In the last decades, the interest of researchers in the development of dense and distributed sensor arrays has grown at a tremendous pace. One of the most promising and ambitious objectives of this research is the development of artificial tactile skins for robotic applications. The reason behind this interest is the huge breakthrough that such a device would represent in many different areas. Lumelsky [1] considers the *sensitive skin* as the missing key device blocking the development of moving machines cooperating with humans in unstructured environments, but highlights its crucial importance also in the fields of prosthetics, industry, wearable computers, and defense.

A complete review on sensitive skins is out of the scope of the present paper (see for example [1]); in this paper we concentrate on three aspects recognized of crucial importance in the design of a generic sensitive skin, as well as on their implications: technology, wiring and processing of sensory data[2].

From the technological side, the sensors integrated so far in sensitive skins can be of very diverse nature: vacuum devices [3], piezoelectric devices [4], micromachined capacitive sensor arrays [5], micromachined inductive sensor arrays [6], resistive sensors [7], accelerometers and piezoelectric strips [8], optical sensors [9, 10, 11], just to cite a few ([1] contains a more complete review of materials and sensors used in sensitive skins).

It is nowadays accepted that a general purpose sensitive skin should be able to collect at least two kinds of tactile information (usually coming from two separated sets of tactile sensors): one with high spatial acuity, for point localization and spatial discrimination, the other to detect spatially diffuse dynamic events such as slip, with high temporal acuity [2, 12, 1]. In the very recent past [13] presented an anthropomorphic fingertip housing Poly-Vinyldene-Fluoride (PVDF) dynamic sensors and strain gages, as well as some preliminary results of their combined use for discriminating different surfaces. Temperature sensitivity is another important sensing modality for sensitive skins [1]. Usually each family of sensors needs specific electronics for driving and data collection.

As the number of sensors increases, wiring issues become important: in case electrical connections are used to convey sensorial data on large surfaces, signals are susceptible to cross-talk and the skin may act as an antenna [1]. Some authors proposed skins in which wireless communications is used, but bandwidth limitations and increase in complexity as the number of elements increases pose serious limitations [14]. Other proposed solutions to minimize the wiring complexity using banks of LC analog filters as sensitive elements, and only three electrical wires as bus, but with the upper limit of 50 sensors.

The strategies used to extract information from the skin are the last issue for which the solutions presented so far mainly differ. They can be gathered into three main groups: serial, mixed or parallel approach.

In serially read skins, the array is scanned, and Multiplexers are used when the

sensing elements are many [3]. The main limitation of this approach is the bandwidth as the number of sensors increases ([15] described a refresh rate of 40Hz, on 256 sensors). In the recent past a sampling rate of 100Hz was obtained on a tactile sensor array of 624 sensing elements [16].

[17] presents an architecture in which a microprocessor every 25 sensors is embedded in the skin, with the aim of gathering signals and packing them on a RS-422 bus. This solution is nevertheless combined with a scanning strategy. This approach has been described also in more recent works [18].

In the parallel strategy, the output of each sensor reaches directly the central processing unit, without intermediate stages consisting in buses, or multiplexing. As it is easy to understand, higher sampling frequencies can be reached, but wiring becomes a major issue [19]. In the recent past hybrid non-scanning strategies were implemented, but with some major limitations in the recoverable shapes [7].

Again, very recent works highlight the importance of the integration of sensors of varying modalities in a sensitive skin [20]. In order to make this feasible, the sensors must "speak the same language". A small *sensory hub*, to be embedded in the skin, able to collect signals from various sensors, and to code them into the same alphabet would be a significant step toward the creation of a real sensitive skin.

In this work we present the design and fabrication of a prototypical *sensory hub*: a versatile module hosting an electro-optical converter and several MEMS sensors, whose peculiar features allow its integration in a sensitive skin.

The requirements of the system and the approach to its design are discussed in section 2, while its description is reported in section 3; the fabrication of some of its parts, as well as the techniques used for hybrid integration of electronic, mechanical, and optical components are described in section 4; section 5 shows the results of the module validation.

2. General Design Issues

The design of the module for applications in a sensitive skin should take into account several aspects, both from the hardware and software viewpoint [1].

- The possibility for the skin of being arbitrarily large and easily "cut" to be adapted to diverse shapes [1] pushed our choice toward a parallel architecture, in which each sensor has its path to the central processing unit, without a data bus.
- As discussed in the Introduction, a skin with parallel architecture generates a potentially huge amount of data, that needs to be properly transferred and processed. To guarantee good performances, a hierarchical architecture of the whole tactile sensory system is mandatory[21, 1]. Figure 1 shows the abstract structure of the complete tactile system that was implemented.
  At the lowest level is the *peripheral system*, the tactile skin, consisting of a set of *modules*, as it will be explained in the following. The upper layers (the *central*

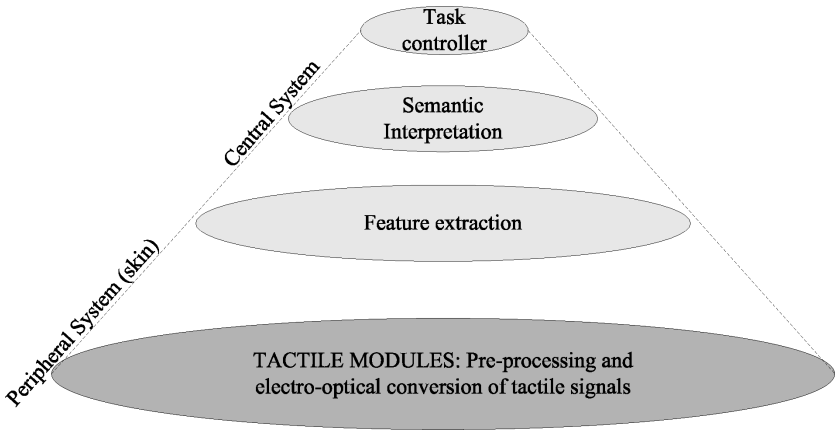

Figure 1. Hierarchical structure of the proposed tactile system. The present work focuses on the lowest level: the skin structure. The upper layers are SW-coded in a small parallel computing architecture, and described in a forthcoming paper.

system) perform tactile feature extraction and, at a more abstract level, their semantic interpretation. The top level of our tactile system houses the controller of the task being accomplished (for instance, a grasp task).
To assure efficient processing of tactile data, special parallel algorithms were developed, and implemented on a VLSI circuit. A thorough description of these algorithms is the object of a forthcoming paper, while here we concentrate on the structuring elements of the peripheral system, i.e. the modules of the tactile skin.
The particular processor adopted accepts images in input: for this reason skin data need to be acquired as *images*. Sensors data are thus converted into the optical domain by the converter, and carried to the processing unit through optical fibres. This solution eliminates cross-talk between signals lines and sensitivity to electromagnetic interferences (EMI).

- As reported in the Introduction, the need for electronics distributed in the matrix is broadly recognized in literature, especially with sensors having many connections, as in the case of silicon multi-axial force sensors, or when different and numerous sensors need to be integrated [1]. The module presented in this paper hosts a digital signal processor with 10 analog input channels with a resolution of 12 bits.
- Flexibility is essential for a sensitive skin, but not for the elementary module [1]; nevertheless a fexible substrate would allow better bending properties of the whole skin. Kapton® was chosen as substrate material for our module: it can hold electronics and mechanics, and can be bent. It can not be stretched, nevertheless the small size of the module, and a careful layout of the wires could overcome this aspect, leaving stretchability to the passive areas of the array. Novel materials were used for flexible stretchable sensitive skins [22], but can not host electronics or sensors other than the ones embedded in the network. As discussed in [23], when the number of sensing elements increases significantly, especially if the number of wires for each sensor is high, the time requested for a complete scan of the matrix would

become unacceptable for many tasks, and the areas of the skin merely devoted to wiring would increase too much.

- As stated in [1], the sampling rate of of a generic control loop involving skin sensors reading, processing, motor commands computation and execution is $30 - 50$Hz. This means that the bandwidth of the skin, a component of the whole sensory-motor control architecture, should be much higher. Moreover, a high bandwidth is necessary to recognize dynamic events, such those arising during slip[24]: biological mechanoreceptors in the human hand skin show their highest sensitivity around 400Hz [25]. In our design each one of the 10 analog channels is sampled at 400Hz.
- In order for the module to be *universal*, i.e., to host different kinds of sensors, it should be programmable; the presence of a digital signal processor (DSP) on-board is essential. Besides adapting the signal conditioning to the particular sensors hosted with the use of several kinds of digital filters, the DSP assures some other prerequisites for a sensitive skin: it selects the essential signals to be sent to the upper layers of the processing chain, by isolating broken sensors, it performs sensors self-calibration and it hosts an automatic gain control function to normalize the array. Moreover, it could be used to extract local features, acting not only as a signals collector and pre-processor, but as a real first layer of processing.
- The density of sensing elements in a sensitive skin is a crucial parameter, related with its spatial performances. We present here a general architecture, that can be easily tailored on specific needs (number, type and geometrical placement of sensors). The specific prototype described in this paper was designed to be integrated in a robotic anthropomorphic hand: it hosts a *strip* of three sensors with a spatial resolution of 5 *mm* and its elongated shape is motivated with the need of wrapping it around the fingers.

3. The module

The primary need that led to the design of the module, was to have a versatile, flexible and miniaturized sensing system capable to 1) acquire sensory signals and optically transmit them; 2) to be extensively integrated in a skin-like structure for robotic tactile applications. Optical transmission was introduced in order to perform high-speed parallel communication immune to electromagnetic interference, and eventually to be able to pack all the transmitted signals in a single optical cable in order to minimize the wiring from the sensor array to the main receiver. The original concept of the module was based on the design of a stand-alone system for each sensor, as represented in figure 2. However, this approach was quickly replaced by the design of a module capable to host more than one sensor and up to nine transmission channels. This choice allows not only to increase the sensor density but also to limit the power and ground connections to all the modules in the array.

The development of a similar module requires the integration of different technologies through several microtechnological processes, leading to a hybrid system

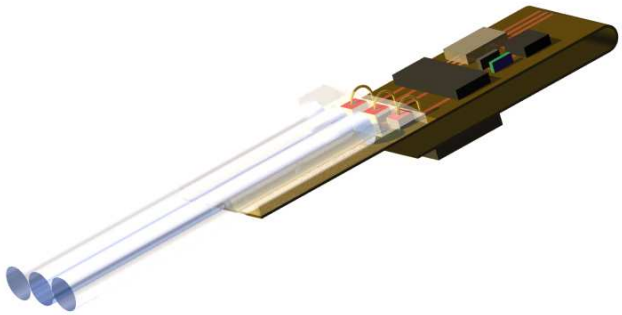

Figure 2. Original concept of a single-sensor module, in particular for a triaxial force sensing MEMS.

which hosts sensors, electronics, and optics on a single miniaturized flexible substrate. These will be described in the following paragraphs.

3.1. Sensors

The module was conceived to host different kinds of sensors. In the present work the circuit layout was designed to host a 3×1 array of three axis force microsensors [26]. The 1.4 mm^3 microsensors are silicon based and high shear sensitive. The 3D structure of one microsensor is shown in figure 3(a). Briefly, the silicon sensor has a high aspect-ratio structure with an integrated silicon mesa used for the transmission of the force to a flexible tethered structure, where four integrated piezoresistors allow to detect the components of an external applied force: in figure 3(a) the locations of the piezoresistors are shown.

When individually considered, from a measure of the four piezoresistors the three components of the applied force can be isolated; nevertheless, the approach followed in this work differs in that these sensors were used to extract *qualitative* rather than *quantitative* information from the input stimulus. Figure 3(b) shows how the piezoresistors were connected; this configuration allows to extract three signals from each sensor: *Vc* is almost proportional to the normal component, while *V13* and *V24* variations are mainly affected by shear components of the stimulus[24]. Without a careful calibration procedure (to be repeated on each sensor) these signals are not rigorously orthogonal, nevertheless they allow the profitable exploitation of the multiaxial characteristics of the sensor itself.

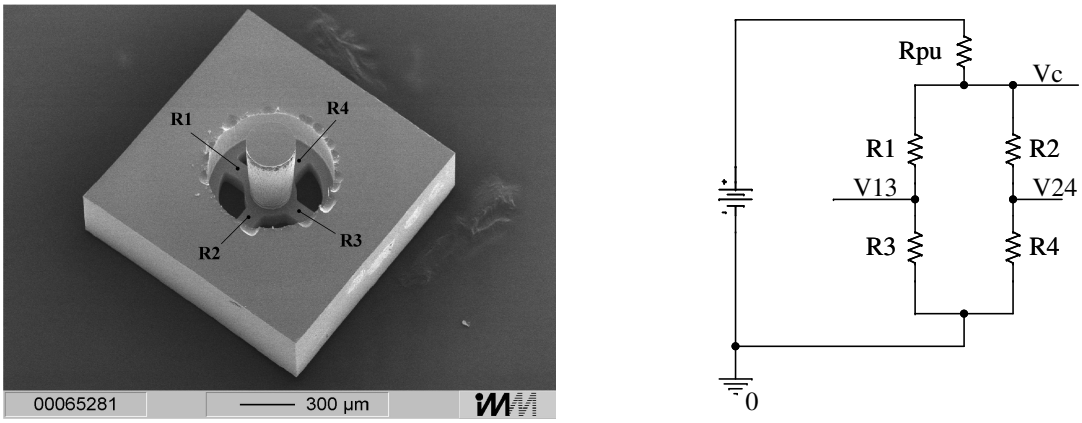

(a) (b)

Figure 3. (a) SEM picture showing the structure of silicon based triaxial force microsensor. Reprinted from [26] with permission from Elsevier; (b) Electrical connections for each of the sensors hosted in the module. *Rpu* is a suitable external pull-up resistor, while *Vc*, *V13* and *V24* are the three signals fed into the dsPIC30F2012 processor (not shown).

3.2. Electronics

The availability of compact and complete digital signal processors allowed to minimize the number of electrical components on the module, whose electronic core is a Microchip dsPIC30F2012: it is a 9×9 mm^2 30 MIPS processor with 10 analog input channels with a resolution of 12 bits and 9 digital outputs, directly connected with the light sources (light emitting diodes, LEDs). Figure 4 highlights the main functional components of the converter, while the algorithm running in the dsPIC is shown in figure 5.

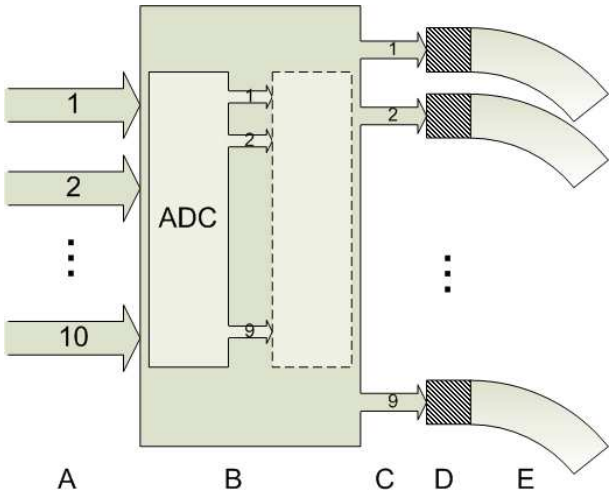

Figure 4. The module can acquire 10 analog voltage inputs (A); inside the dsPic, analog-to-digital conversion is performed, as well as all the signal processing (B); 9 digital pulse-width modulated signals (C) are generated and used to directly drive the LEDs (D); a plastic optical fibre (E) is connected to each LED and propagates the signal to the processing unit (not shown).

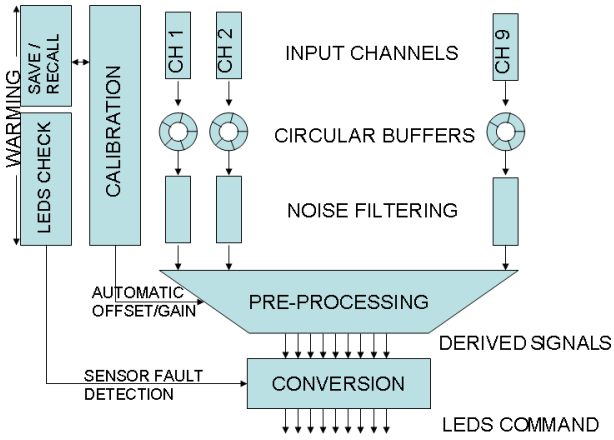

Figure 5. Diagram describing the main components of the converter software architecture. The input signals (CH1 - CH9) are sampled at the rate of 400Hz and fed into 9 circular buffers. A noise removal filter is applied and then a pre-processing phase extracts significant information from the signals. In this phase automatic and adaptive gain and offset regulations are performed: an initial calibration, performed during the so called *warming phase*, is therefore necessary, and the results are stored in the non-volatile memory for use at each start-up. LEDs are driven by nine pulse-width modulated signals, generated in the conversion phase. LEDs corresponding to broken input channels, which are automatically detected during startups, are isolated.

The analog-to-digital conversion runs continuously in background, and the system clock triggers the filling of 9 circular buffers at a rate of 400Hz. Each circular buffer contains 5 samples of the corresponding channel, thus keeping a history of the past 12.5 ms on each channel. The dsPIC could allow a sampling rate four times higher: the chosen value results from a trade off between required performances and power consumption.

A digital filter is then applied to each channel in order to lower the noise coming from the sensors. Noise removal is a crucial aspect in sensor data processing: the correct approach depends on the kind of sensor being used, and the dsPIC can perform moving averages, as well as polynomial, finite impulse response (FIR) or infinite impulse response (IIR) filtering on the samples contained in the buffers. This is an important feature in order to increase the general purpose characteristics of the converter.

When multiple sensors are to be used, calibration is essential. It is extremely rare that three sensors with the same nominal characteristics behave at the same manner. Therefore, the module implements three different calibration procedures, to adapt to user's needs:

- Static calibration: this procedure equalizes static differences among the channels when no stimulus is applied.
- Basic dynamic calibration: this procedure performs a series of measures on each channel with no stimulus and with a static stimulus, equalizing offset and dynamic range of each channel. A measure of the standard deviation on each channel is then used as indicator of the signal-to-noise ratio and used in the noise filtering

procedure, which, in this way, becomes adaptive.

- Advanced dynamic calibration: with respect to the previous case, the measures are taken without stimuli, and with stimuli varying over time, the same for all the sensors mounted on the module (this modality obviously implies that the same kind of sensors is used). This modality verifies and improves the linearity of the converter's response.

The output of the calibration phase consists of a set of values used for automatic offset and gain control of the sensor array, and is saved in the dsPIC's non-volatile memory, so that the procedure does not need to be executed at each startup. A remote key allows the user to force a static calibration at any time, while the other two types of calibration must be chosen during the warming phase, the initial 4 s after startup.

Another important function implemented in the converter during the warming phase is the *sensors check*, i.e., the search for not working channels. The checks to be performed to inquiry the status of a sensor depend on the sensor type. The current implementation considers three cases for fault detection: sensor output tied to supply voltage, to ground, or to a voltage significantly different with respect to the one stored in memory during the first calibration. Channels recognized as not working are isolated and the corresponding light emitters are shut down.

The pre-process phase, which extracts, from raw sensory data, meaningful information (*derived signals* in figure 5) to be coded into optical signals, highly depends on the sensors hosted on the module. In this case, differences between the actual values and the corresponding ones stored during the *warming* phase are used.

During the conversion phase, derived signals are coded into pulsed signals, used to directly drive the light emitters. In order to obtain continuous light intensity modulation using digital outputs from the dsPIC, light emitters are actually driven in Pulse Width Modulation (PWM) mode: the duty cycle of the square digital signal (whose frequency is 400Hz) that drives each led is proportional to the value of the corresponding *derived signal*.

Each channel uses an independent counter to adjust the duty cycle, so that the same procedure can be used at the same time for different sensors, preserving the modulation index even with diverse dynamic ranges.

3.3. Optics

The optical system in the converter has the role to convert PWM voltage signals, coming from the dsPIC, in optical radiation to be coupled into plastic optical fibres (POFs), which waveguide signals up to the detector. Primary requirements for the whole transducing system are ease of fabrication and assembly, in order to be reproducible with medium (or mass) production, low cost and robustness. All its sub-modules need to accomplish with these requirements, in particular optics. Optics allows a high degree of integration and signal coding. An outstanding feature optics can introduce, in such an application, is signal transmission with Wavelength Division Multiplexing (WDM)

strategy, in order to transmit at different wavelengths all the electro-optical transduced signals to the final detector through a single optical fibre. The different spectral components of the light transmitted would undergo spatial separation at the front-end by means of a standard (or eventually miniaturized) spectroscope. In conclusion, with a single thin cable it would be possible to transmit at the same time information from many sensors, at very high speed and avoiding any problem connected with external electromagnetic interference.

However, in order to validate the concept of the module and its overall performances, and, at the same time, limit the technological efforts and costs, a simpler converter was fabricated, where for each light emitter (i.e., channel) a fibre was connected to the optical part. As a consequence, a single optical signal propagates undisturbed in each fibre and this allows the use of spectrally identical light sources.

Three possible solutions were considered regarding light sources:

- Surface-Emitting Light Emitting Diode (SE-LED): light is emitted upward with a typical lambertian radiation pattern. SE-LED dies are easy to find commercially at low cost and in a wide range of sizes and spectral characteristics.
- Edge-Emitting LED (EE-LED): the light is emitted from the side wall of the LED. The light spot is much more focused, and the side emission allows a direct and more efficient coupling of the light into the fibre. The principal drawbacks are higher costs, the fact that on-chip precise alignment processes are required and higher input currents compared to SE-LEDs.
- Vertical-Cavity Surface-Emitting Laser (VCSEL): it is a surface emitting micro-LASER commercially available in dies and already packed in arrays of several units with extremely low threshold currents (less than 1 mA) and extremely narrow beams.

The first prototype presented in this paper uses the most common and cheap SE-LEDs to be mounted on the substrate. In order to keep the whole module system as much flat as possible, in order to be embedded in a skin-like package as the present application requires, a system able to redirect the light emitted mainly vertically from the SE-LED needs to be integrated. For this purpose, a metallic micro-mirror was fabricated with micromachining processes. The first mirror prototype was conceived for a compact converter with only three channels but it was quickly replaced by a larger structure conceived for nine channels and capable to suppress, or drastically limit, the cross-talk between channels, as it will described in the following.

Therefore, the final optical system includes:

- Nine SE-LEDs. Commercial LED dies, ELC-660-23 from Epigap, were used. They emit radiation with a wavelength of about 650 nm (visible red) and they have a size of $275 \times 275 \times 180$ μm^3;
- A metallic case, with a size of $6.5 \times 4 \times 1$ mm^3, which has the role of:
  - Reflecting the light emitted by LEDs into the POFs, by mean of a 45°-mirror inside the metallic case;

  - Preventing or drastically reducing the cross-talk between the optical channels, due to an interleaved placement of the front-end of the POFs;
  - Packaging the POFs and protecting LEDs and bonding wires;
  - Conferring robustness to this delicate part of the converter.

- Nine Poly-Methyl-Meta-Acrylate (PMMA) POFs with a diameter of 500 μm and a length of about $1.5 - 2$ m. Conventional POFs are much worse than glass fibres regarding optical transmission efficiency. The POFs used have a loss of $0.15 - 0.2$ dB/m at 650 nm and the transmission bandwidth is limited by their large numerical aperture (NA) and step-index profile. However, they are adequate for running short links, such as inside instruments or within a room for desktop connections up to 50 meters. The small distances to be covered in the present application make the power loss along the fibre a negligible problem. Nevertheless, coupling the light into the fibre is a major issue.

  In figure 6 a complete CAD model of the optical part is shown.

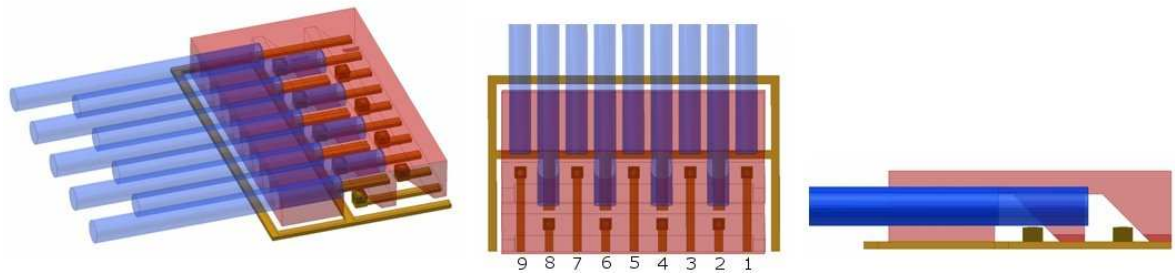

Figure 6. 3D CAD model of the optical architecture for nine channels; the metallic case has been drawn partially transparent for a better understanding of the underneath structure and devices; bonding-wires of the LEDs are not shown.

The optical structure has been developed for two prototypes, with minor changes. The first prototype was fabricated on a separated Kapton® substrate and afterward connected to the main electronic module through a zero insertion force (ZIF) connector, see figure 7.

The second prototype of the optical structure was assembled directly on the same flexible substrate, where electronics and sensors were assembled too, figure 8. The metallic case was also covered by a thin film of insulating paint to avoid any possible short-circuits with the underneath electrical lines. Please, refer to the next Section 4 for a detailed description of the fabrication and assembly steps of the optical part.

4. Parts fabrication and module assembly

The most crucial aspect of the module fabrication is that several different devices and structures need to be assembled on a small piece of flexible substrate using different technologies and processes, which can also affect each others. The fabrication is organized in four main consecutive steps:

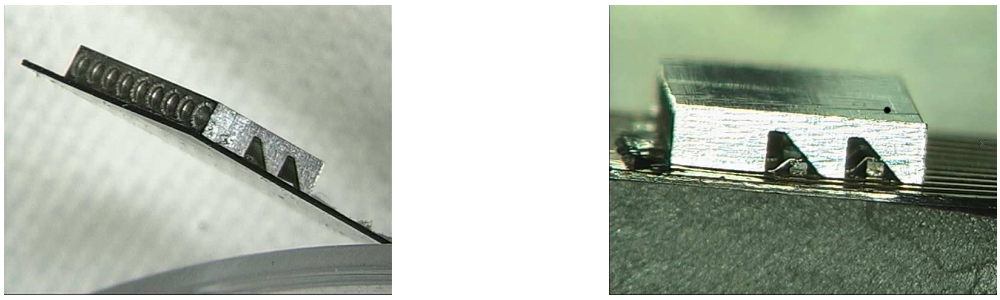

(a) (b)

Figure 7. (a) First stand-alone optical structure on Kapton® substrate, to be connected to the electronic part through a micro ZIF connector; (b) Wire-bonded LEDs are visible under the mirror structure.

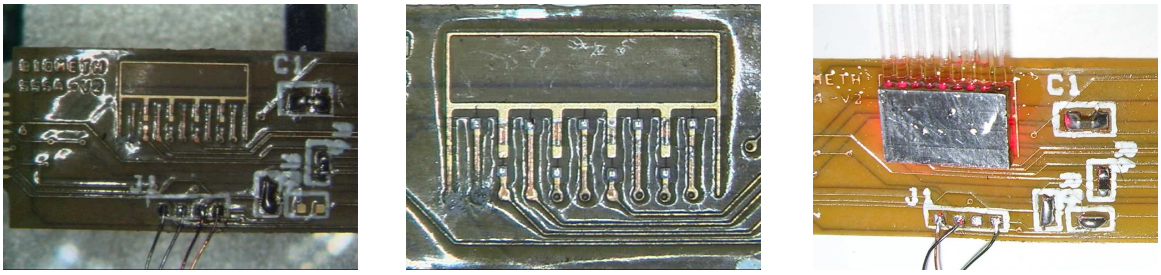

(a) (b) (c)

Figure 8. (a),(b) Final flexible substrate: assembly area of the optical part, LEDs are already assembled and wire-bonded; (c) Optical part completely assembled in a module prototype.

- standard integration of surface mounted electronics;
- assembly of the three sensors and packaging;
- assembly of optics;
- dsPIC programming, calibration and test phase.

4.1. Electronics

Commercial electronics was used in the converter. Six resistors, three capacitors and one dsPIC were surface mounted directly on the Kapton® substrate by soldering. More than 40 substrates were prepared with assembled electronics.

4.2. Sensors array

The fabrication and assembly of the 3×1 flexible tactile sensor array has been performed by means of the same approach followed in [24]. In such previous work a Soft Complant Tactile Microsensor (SCTM) has been developed integrating one silicon triaxial microsensor into a soft, compliant, flexible but robust packaging. The packaging of the microsensors array consisted in two main parts, i.e. the contact of the microsensors

to flexible connections and the implementation of a mechanical compliant interface between the sensor and the outer world.

The microsensors were mounted on the flexible circuit exploiting the 5552 R Z-Axis Adhesive Film (3M, St. Paul MN, USA) by means of a curing process. In order to finely align and place sensor pads onto the Kapton® pads a specifically-conceived assembly station was used (figure 10(a)). The station gives the capability to precisely control the position of the sensor to be assembled in the x-, y- and z-axis plus rotation around the z-axis and tilt angle control around the x- and y-axis. The z-axis itself is motorized with a computer controlled motor stage with sub-μm resolution. The sensor was held by a suction pipette, which is joined to a load cell (precision miniature load cell 31 by Honeywell Sensotec) monitored by computer, used to control the correct pressure applied on the sensor during the curing process. The Kapton® substrate was fixed on a heated plate, whose temperature is also monitored by the computer. As only one sensor could be assembled at a time, and relaxation of the tape could be induced by substrate re-warming (decreasing the electrical conductivity and mechanical adhesion), it was essential to create a thermal barrier between the curing sensor and the assembled ones: a thermoelectric Peltier module was placed besides the heated plate, obtaining a 110°C gradient between two adjacent sensors.

Figure 9 shows the area of the circuit housing the sensors, as well as the three force microsensors assembled on the module, before and after a mechanical compliant interface made of polyurethane (Poly 74-45 from PolyTek, USA) was poured on them. The thickness of the polyurethane layer is 2 mm.

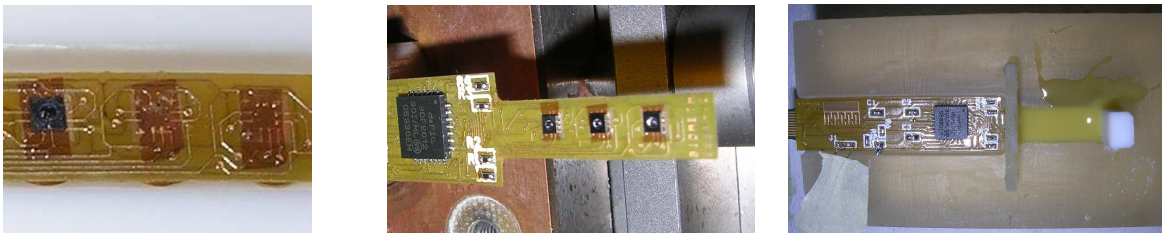

(a) (b) (c)

Figure 9. (a) Detail of the part of the module hosting the sensors; the triaxial force sensors are visible on the module, before (b) and after (c) soft polyurethane casting in the plastic mould.

4.3. Optics

The optical part is the last to be assembled on the flexible substrate and it requires time-consuming processes, since no automatic assembling machines were used (currently not available among lab's facilities) for mounting the optoelectronic devices. Nevertheless, the entire process of fabrication and assembly of the optical part is feasible with automatic machines for mass production. Hereafter a short description of the fabrication process is reported.

After cleaning with Acetone the electrical pads of the optical part, the substrate was placed in the same assembly station used for the sensors, figure 10(a), and fixed through small magnets to the metallic plate, figure 10(b).

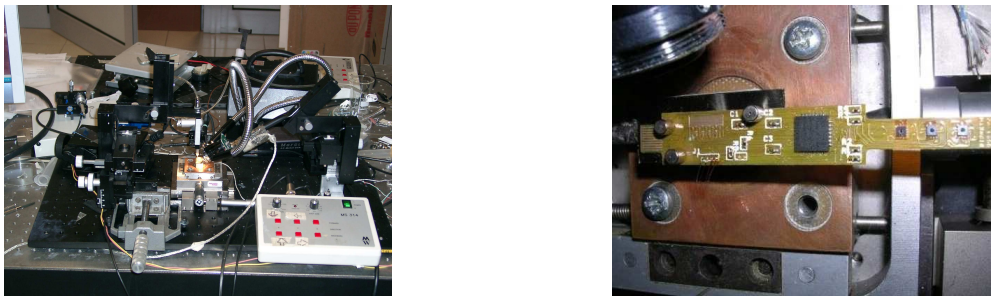

(a) (b)

Figure 10. (a) Laboratory-made assembly station used to mount small devices onto the Kapton® substrate; (b) The flexible substrate with electronics and sensors already mounted and ready for assembly of optical part.

First process step consisted of dispensing an electrically conductive die attach adhesive (Ablestik 84-1LMISR4) by a custom pipette with an inner hole diameter of about 200 μm, which is directly connected to a pneumatic dispenser. The process was repeated for all the nine pads and required a fine control of the glue releasing in order to avoid short-circuits between close electrical lines, whose distance can be less than 300 μm. Placement of LEDs on the pads followed, refer to figure 11(a). This was accomplished using another small pipette, which was connected to a pump in order to have suction capability. Each LED was grasped by suction and transported on the glue drop, it was visually aligned with pad and finally pressed slightly down on it. The pump was switched off and after waiting about one minute the pipette was lifted up, while the LED remained glued to the pad. After completing this procedure for all the LEDs, the flexible substrate was inserted into an oven and heated at about 150°C for about one hour in order to cure the conductive glue. Finally, the module was placed in the wire-bonding machine, where all the LED top electrodes (cathodes) were bonded to the front pad, which is electrical ground, see figure 11(b). Particular attention was devoted to maintain the height of the bonding-wire loop very low, in order to avoid to break bonding wires during placement of the metallic case. All the described processes for LED mounting can be re-defined to fulfill with industrial automatic machines requirements, in order to achieve mass production.

Before mounting the metallic case, LEDs were tested, see figure 11(c).

The metallic case, in figure 12, was fabricated through two different micromachining processes. The initial rough metallic block was prepared with conventional milling machines. The holes for fibres insertion were created as first by a 5-axis ultra-precision Kern CNC machine, using a drilling tip with 550 μm diameter, 50 μm more than the nominal diameter of the optical fibre, in order to compensate for optical fibres tolerances. Afterward, the metallic part underwent micromachining in a micro-wire

(a) (b) (c)

Figure 11. (a) LED alignment and assembly on the pad with the glue drop already placed; (b) Wire-bonded LED (consider the LED is only 180 μm thick); (c) Test of LEDs mounted on the flexible substrate; note the metallic case on the right ready for being assembled. The two visible metallic sticks are the probes of a multimeter used to test the LEDs.

Electro-Discharging-Machine (EDM AP200L from Sodick), where the two 45°-inclined mirror sides were formed. A nine-passes process was selected, using a brass-coated piano wire with a diameter of 100 μm. The double stage mirror was conceived in order to prevent, or drastically limit, cross-talk between close channels, since all the LEDs emit at the same wavelength and, consequently, the signal could not be distinguished or separated at the receiver. The profile of the mirror can also be parabolic shaped in order to have a higher focusing of the light toward the fibres. Depending from the material, very low roughness of the mirror can be achieved with EDM machining. In the developed prototype an aluminum alloy (Ergal) was used in place of more performing materials, such as steel or brass, for instance, mainly because the manufacturing process was faster and cheaper. Measurements of the surface roughness of the mirror side of the metallic case gave an Ra of around 0.27 μm on a 1 mm-long span of the testing probe, please refer to section 5. The design and fabrication of the metallic case were also performed in a way to form a mechanical end-stop to fibres during insertion, in order to prevent fibres going against and breaking the bonding wires of the LEDs, see figure 12(b) and also figure 13(a), where a close view of the bottom side of the metallic case is shown.For a larger magnification see also figure 15(a). The metallic end-stops shield light from coupling into the fibres for just a very small percentage. The thickness of the end-stops was calculated taking into account the nominal tolerances of the POF diameter.

Currently, the conceived fabrication process allows to produce ten metallic cases in a single machine run.

Before assembly, the metallic case and, in particular, the mirror sides were cleaned with acetone and by ultrasonic bath to remove dirt, mainly due to the erosion process in the micro-EDM. Mounting of the metallic case was performed in the assembly station using a larger suction pipette, see figure 13, and monitoring the pressing load onto the substrate with the precision load cell. The metallic case was glued on the substrates with non-conductive epoxy glue.

Finally, the POFs were cut, perpendicularly to their axis, with a a standard blade

(a) (b) (c)

Figure 12. (a) Bottom view of the metallic case, shown with fibres already inserted in the holes before assembly just to demonstrate their disposition; (b) Front view showing the nine holes fabricated by micro-drilling for hosting the POFs; mechanical end-stops can be distinguished at the end of the five shorter holes (c) Side view: the two 45°-sloped mirrors are clearly visible.

(a) (b) (c)

Figure 13. (a) Close view of the bottom side of the metallic case; (b) Metallic case held by the suction pipette in the assembly station; (c) The metallic case is finely aligned and placed onto the LEDs.

cutter, and they were manually inserted with no particular attention (the mechanical end-stops prevent any damages to the optoelectronic devices) and fixed to the metallic mirror with few drops of epoxy glue. Glue self-distributed among the POFs for capillarity.

In figure 14 the final assembled module is shown, alone and applied to the fingertip of a robotic hand.

5. Tests

A series of tests were conducted on the module, on its optical and electrical parts. This section summarizes the methods, the results and a brief discussion.

5.1. Electro-optical converter

The coupling efficiency between the LEDs and the fibres, as well as the optical cross-talk introduced by the device, are crucial factors for a good electro-optical conversion. While the former mainly follows from placement inaccuracies during the assembling phase of LEDs and mirror, the latter is intrinsic to the mirror structure, in particular to its

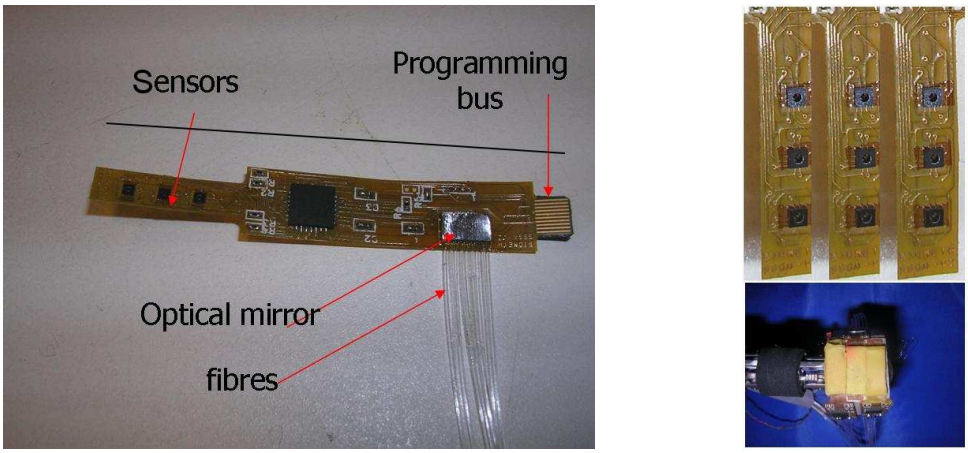

(a) (b)

Figure 14. (a) Unpackaged prototype of the module. The black line is 6 cm long; (b) Application of three modules to a robotic hand finger: uncovered sensor array (top) and complete finger.

design and the smoothness of its machined surface. Since the cut of the plastic optical fibres was manually performed, the section of the fibre termination could slightly differ from fibre to fibre. This can imply a different efficiency in light coupling and emission. Therefore, the same probing fibre was used to measure cross-talk between channels, during the tests. The light intensity was measured by connecting the probing fibre with a Vishay BPW34 photodiode. The generated photo-currents were converted into voltages by means of a simple resistive network and measured using a Fluke 190C digital oscilloscope. The effects of a not perfect alignment between the LEDs and the fibres are significant: each of the nine LEDs was powered, one at a time, and the emitted light was measured at the end of the probing fibre for each channel; the average standard deviation in emission intensity among all the LEDs, measured at the end of the probing fibre resulted to be about 10.8%. An automatized assembling of the components (LEDs and metallic case) would certainly allow more accurate placements and thus a more uniform emission between the channels.

The amount of optical cross-talk introduced by the mirror itself was also measured. The test was performed turning a single LED on at full power, and measuring the coupled light into the adjacent channels with the probing fibre. Cross-talk measurements are given in percentage on the value of the current, generated by the photodiode, obtained by probing the light of the emitting LED in its own channel (maximum intensity). Two versions of the metallic case were compared: the first was an originally built metallic case with a single-stage mirror and all the fibres aligned with the same length (as in the simple concept of figure 2), with a diameter of only 250 μm and placed at a distance of 0.7 mm between each other (measured between their section centers); the second was the metallic case of figure 6 with fibres with interleaved lengths, and a diameter of 500 μm, always placed at a distance of 0.7 mm between each other. The measure was repeated for each of the nine LEDs, and with each of the adjacent channels.

The first metallic case showed a significant cross-talk of about 12.6% between two adjacent fibres, while, in the second prototype, the maximum measured cross-talk was reduced to 1.1%. Consider also that fibres in the second mirror version have a two-times larger diameter than those in the first mirror version, which is a conservative feature from the viewpoint of the cross-talk dynamics. As expected, in the metallic case of figure 6, the maximum value was measured between two adjacent channels belonging to the second mirror stage (i.e., between fibres 2 and 4, 4 and 6, 6 and 8, in figure 6). However, cross-talk between adjacent fibres that collect the light from the first mirror stage (fibres 1, 3, 5, 7, 9) was almost the same of adjacent fibres collecting the light of the second mirror stage. A dark-paint coating of the terminal parts of fibres 2, 4, 6 and 8 would probably better prevent cross-talk between the channels 1, 3, 5, 7, 9.

Further tests in which the probing fibre was in different positions (1, 2, .., 9) demonstrated the constancy of the cross-talk performances between all the mirror channels.

The prototypes described in this paper were fabricated in ERGAL Aluminum alloy, whose superficial roughness contribute to the residual cross talk that was measured. The surface rugosity of the samples was measured by means of a Surfcom 130A from TZK-Zeiss rugosimeter: a $Ra = 0.27 \pm 0.03\ \mu m$ over a $1\ mm$ horizontal span was found. A similar test performed on a piece of steel machined with the same EDM process highlighted an average rugosity $Ra = 0.20\ \pm\ 0.02\ \mu m$. In figure 15 two images of the aluminum mirror surface, generated by detailed inspection with Focused Ion Beam (Fei FIB 200 Workstation), are shown.

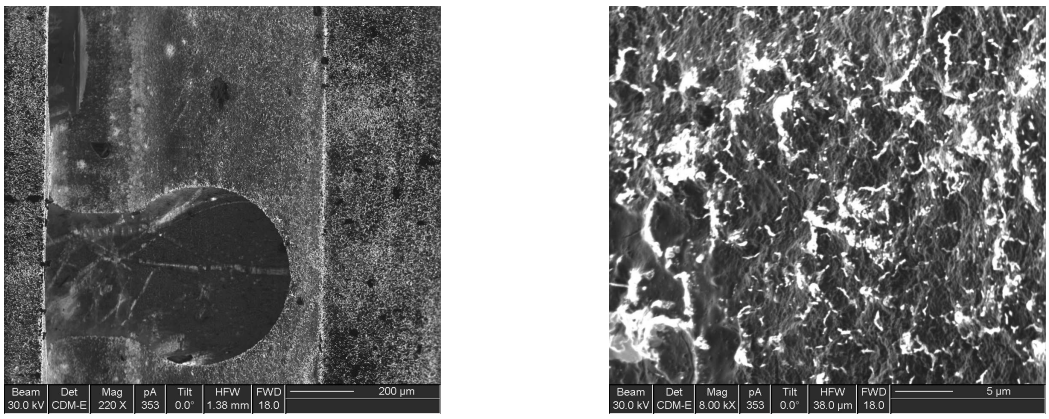

(a) (b)

Figure 15. (a) Close FIB view of the first stage mirror; (b) Magnification of the mirror surface.

5.2. Complete module

A six-components load cell (ATI NANO 17 F/T, Apex, NC, USA) was mounted in the same test bench used for positioning the micro-mirror. An aluminum-fabricated low-curvature loading probe, attached to the load cell, was used to apply the stimulus

normal to the sensors. The loading force corresponding to the leds activation threshold was digitally recorded (using a National Instruments USB-6008 acquisition board). An average activation pressure threshold of $1.7mN/mm^2$ was achieved.

A mini-shaker (Brüel & Kjaer model 4810) equipped with a cylindrical probe (with diameter of 1mm) was used to apply sinusoidal stimuli to the packaged sensors, orthogonal to the sensors themselves. The amplitude of the oscillating stimulus, equal to the superficial indentation of the polyurethane packaging, was measured through a non-contact laser sensor (micro-epsilon optoNCDT 1401) focused on the probe. A Vishay BPW34 photodiode was coupled to the optical fibre corresponding to the *Vc* signal (see figure 3) of the stimulated sensor, and a simple resistor was used to obtain a voltage signal, proportional to the incident light. These signals were digitally acquired at $1k$Hz sampling rate by means of a National Instruments USB-6008 acquisition board.

The minimum indentation that could be detected by the module was equal to $200\mu m$: this value was used in the dynamic measures. Figure 16 summarizes the results of two acquisitions, at 20 and 50 Hz: the two curves are the ratios between the output (light) and input (indentation) power spectra. The low frequency components are due to the fact the resting height of the probe (the average amplitude of the oscillation) was set very close to the indentation threshold. Results show that the the stimuli are correctly converted in the module.

Complete static and dynamic characterizations of the module, allowing the extraction of its full frequency response, are future work.

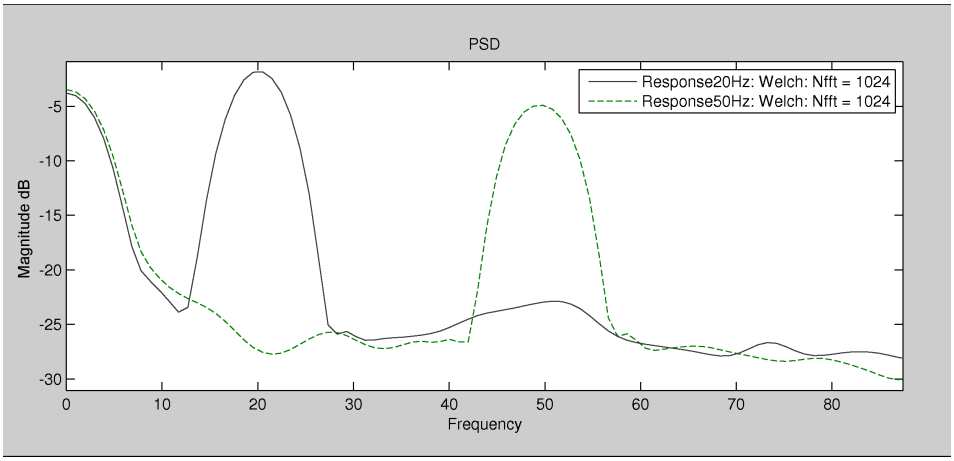

Figure 16. Partial frequency response of the module, corresponding to two sinusoidal stimuli at 20 and 50 Hz.

Figure 17 shows three tactile images generated by an array of 3 modules with three different tactile stimuli: each blob corresponds to an optical fibre.

6. Conclusions

A miniaturized electro-optical sensing module was designed and fabricated to be used in the peripheral sensitive layer of a complete artificial tactile system; the first developed

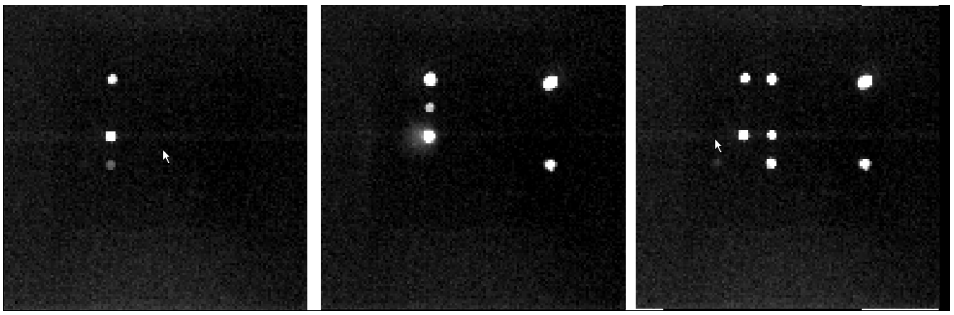

Figure 17. Three tactile images from a small array of modules.

prototypes, presented in this paper, aimed at validating the approach, based on the optical parallel and EMI-immune transmission of locally and adaptively preprocessed signals to the upper layers of the tactile system.

The paper describes the design of the module, as well as its microfabricated parts, and the hybrid processes necessary for its assembly. Technical solutions to serially build several prototypes are presented.

The design criteria, which allow the pervasive employment of the module for the fabrication of two-dimensional arrays of sensing structures (e.g., *sensitive skins* [1]) were met: its flexible substrate can be shaped depending on the application requirements; the programmable processor on board makes it suitable for the simultaneous use of different sensors; the maximum available bandwidth of the converter (400Hz per channel in the current implementation) allows detection of sudden events; the resolution of the analog-to-digital conversion and the automatic gain and offset controls allow optimal adaptation to sensors having different dynamic ranges; the optical coding assures transmission of information immune to EMI; the mechanical design and fabrication solutions adopted for the optics assure extremely low cross-talk between the optical fibres, while minimizing the size of the device.

In particular, in the application presented in this paper: the module was shaped to be wrapped around the fingers of a robotic hand and hosts three MEMS force sensors in the fingertip area; an overall minimum bandwidth of 50Hz was measured, limited by the protective polyurethane package; a pressure sensitivity of 1.7 mN/mm^2 was measured; the minimum detected indentation was 200 μm.

Current activity is devoted to optimize the packaging of the sensors (i.e., material, thickness, surface characteristics) in order to 1) maximize bandwidth, linearity, and sensitivity of the module while guaranteeing flexibility and protection of the sensors; 2) to increase the integration of the electronics according with improved module shapes. Application of Wavelength Division Multiplexing to drastically reduce the number of optical fibres, while maintaining the transmitted information density, is being investigated.

Acknowledgments

The authors wish to express their gratitude to Mr. Carlo Filippeschi and Mr. Riccardo Di Leonardo for their skilled help in assembling the sensors and the electronics, and to Mr. Alessandro Persichetti for assembling the test bench used for dynamic measures. The work described in this paper was carried on in the framework of the BIOMETH (Biomimetic Touch and Sight) project, supported by Toyota Motor Corporation. A special thank goes to Mr. Hiromichi Yanagihara and Mr. Jonas Ambeck-Madsen from Toyota Motor Europe for the many fruitful discussions and the continuous support.

References

[1] V.J. Lumelsky, M.S. Shur, and S. Wagner. Sensitive skin. *Sensors Journal, IEEE*, 1(1):41–51, 2001.

[2] R. D. Howe. Tactile sensing and control of robotic manipulation. *Journal of Advanced Robotics*, 8:245–261, 1994.

[3] Z. Wen, Y. Wu, Z. Zhang, S. Xu, S. Huang, and Y. Li. Development of an integrated vacuum microelectronic tactile sensor array. *Sensors and Actuators A*, 103:301–306, 2003.

[4] P. Li and Y. Wen. An arbitrarily distributed tactile piezoelectric sensor array. *Sensors and Actuators A: Physical*, 65(2):141–146, 1998.

[5] BL Gray and RS Fearing. A surface micromachined microtactile sensor array. *Robotics and Automation, 1996. Proceedings., 1996 IEEE International Conference on*, 1, 1996.

[6] N. Futai, K. Matsumoto, and I. Shimoyama. A flexible micromachined planar spiral inductor for use as an artificial tactile mechanoreceptor. *Sensors and Actuators A: Physical*, 111(2-3):293–303, 2004.

[7] H. Zhang and E. So. Hybrid resistive tactile sensing. *Systems, Man and Cybernetics, Part B, IEEE Transactions on*, 32(1):57–65, 2002.

[8] R. D. Howe and M. R. Cutkosky. Sensing skin acceleration for slip and texture perception. In *Proceedings of the 1989 IEEE International Conference on Robotics and Automation*, pages 145–150, Scottsdale, Arizona, May 1989.

[9] O. Tohyama, S. Maeda, and H. Itoh. Fiber-Optic Tactile Microsensor for Detecting the Position of the Tip of a Fiberscope. *IEEE Journal of Selected Topics in Quantum Electronics*, 5(1):115, 1999.

[10] H. Maekawa, K. Tanie, and K. Komoriya. A finger-shaped tactile sensor using an optical waveguide. *Systems, Man and Cybernetics, 1993.'Systems Engineering in the Service of Humans', Conference Proceedings., International Conference on*, pages 403–408, 1993.

[11] G. Kinoshita, Y. Kurimoto, H. Osumi, and K. Umeda. Dynamic contact sensing of soft planar fingers with tactile sensors. *Robotics and Automation, 2001. Proceedings 2001 ICRA. IEEE International Conference on*, 1, 2001.

[12] HR Nicholls and MH Lee. Tactile sensing for mechatronics—-a state of the art survey. *Mechatronics*, 9:1–32, 1999.

[13] K. Hosoda, Y. Tada, and M. Asada. Anthropomorphic robotic soft fingertip with randomly distributed receptors. *Robotics and Autonomous Systems*, 54(2):104–109, February 2006.

[14] H. Shinoda and H. Oasa. Wireless tactile sensing element using stress-sensitive resonator. *Mechatronics, IEEE/ASME Transactions on*, 5(3):258–265, 2000.

[15] O. Kerpa, K. Weiss, and H. Worn. Development of a flexible tactile sensor system for a humanoid robot. *Intelligent Robots and Systems, 2003.(IROS 2003). Proceedings. 2003 IEEE/RSJ International Conference on*, 1, 2003.

[16] H. Kawasaki, T. Komatsu, and K Uchiyama. Dexterous anthropomorphic robot hand with

distributed tactile sensor: Gifu hand ii. *Mechatronics, IEEE/ASME Transactions on*, 7(3):296–303, Sept 2002.

[17] H. Odeberg. A tactile sensor data-processing system. *Sensors and Actuators A*, 49:173–180, 1995.

[18] Y. Xu, Y.C. Tai, A. Huang, and C.M. Ho. IC-Integrated Flexible Shear-Stress Sensor Skin. *Journal of Microlectromechanical Systems*, 12(5), 2003.

[19] A. Jimenez, A. Soembagijo, D. Reynaerts, H. Van Brussel, R. Ceres, and Jl Pons. Featureless classification of tactile contacts in a gripper using neural networks. *Sensors and actuators. A, Physical*, 62(1-3):488–491, 1997.

[20] WD Stiehl, L. Lalla, and C. Breazeal. A "somatic alphabet" approach to "sensitive skin". In *Robotics and Automation, 2004. Proceedings. ICRA'04. 2004 IEEE International Conference on*, volume 3, 2004.

[21] SC Jacobsen, ID McGammon, KB Biggers, and RP Phillips. Design of tactile sensing systems for dextrous manipulators. *Control Systems Magazine, IEEE*, 8(1):3–13, February 1988.

[22] T. Someya, Y. Kato, T. Sekitani, S. Iba, Y. Noguchi, Y. Murase, H. Kawaguchi, and T. Sakurai. Conformable, flexible, large-area networks of pressure and thermal sensors with organic transistor active matrixes. *Proceedings of the National Academy of Sciences*, 102(35):12321–12325, 2005.

[23] J. Engel, J. Chen, Z. Fan, and C. Liu. Polymer micromachined multimodal tactile sensors. *Sensors and Actuators A*, 117:50–61, 2005.

[24] L. Beccai, S. Roccella, L. Ascari, P. Valdastri, A. Sieber, M.C. Carrozza, and P. Dario. Experimental analysis of a soft compliant tactile microsensor to be integrated in an antropomorphic artificial hand. In *Proceedings of ESDA 2006, 8th Biennal ASME Conference on Engineering Systems Design and Analysis*, 2006.

[25] E.R. Kandel, J. H. Schwartz, and T.M. Jessel. *Principles of Neural Science*. Mc Graw Hill, fourth edition edition, 2000.

[26] L. Beccai, S. Roccella, A. Arena, F. Valvo, P. Valdastri, A. Menciassi, M.C. Carrozza, and P. Dario. Design and fabrication of a hybrid silicon three-axial force sensor for biomechanical applications. *Sens. Actuators, A*, 120:370–382, 2005.